SYNTHESIS OF FeAPO-34 MOLECULAR SIEVE UNDER IONOTHERMAL CONDITION

Mazlina Musa[a,b*], Daniel M. Dawson [b], Russell E. Morris [b], Sharon E. Ashbrook [b]

[a]Department of Chemistry, Faculty of Science and Mathematics, Sultan Idris Education University, 35900, Tanjung Malim, Perak, Malaysia

[b]School of Chemistry, EaStCHEM and Centre for Magnetic Resonance, University of St Andrews, North Haugh, St Andrews KY16 9ST, Scotland, UK

Corresponding author email: mazlinam@fsmt.upsi.edu.my

Abstract

FeAPO-34 with chabazite (CHA) topology structure was successfully synthesized under ionothermal conditions using 1-ethyl-3-methylimidazoliumchloride (EMIMCl) ionic liquid in the presence of ethylenediamine (EDA). The material was characterised using powder Xray Diffraction (XRD), thermogravimetric analysis (TGA), elemental analyses and solid-state NMR spectroscopy. Incorporation of iron within the covalent framework of the material was confirmed by the presence of broad signals between 1000 and 14000 ppm in the ^{31}P NMR spectrum, corresponding to $P(OFe)_x(OAl)_{4-x}$ species.

Introduction

Zeolite and zeotype molecular sieves are widely used as catalysts, gas adsorbents, and ion exchangers in many industrial applications.[1-3] Aluminophosphates (AlPOs) are family of zeotype that have similar microporous framework structures to zeolite, but cannot be used directly as

catalysts since their frameworks comprise strictly alternating AlO_4 and PO_4 tetrahedra, forming a neutral framework charge resulting in a lack of acid sites. This feature can be improved by aliovalent substitution of Al^{3+} or P^{5+} with other heteroatoms such as Si^{4+}, Mg^{2+}, Co^{2+}, Mn^{2+}, Zn^{2+}, etc. to produce silicoaluminophosphates (SAPOs) or metalloaluminophosphates (MAPOs), respectively. Inserting heteroatoms into the AlPO framework generates a negative charge, compensated by H^+ to form strong acid sites, thereby creating potential solid-acid catalysts.[2] Conventionally, AlPOs are synthesized using hydrothermal or solvothermal methods under high autogenous pressure where a molecular liquid is used as the solvent and organic cations (structure directing agents, SDAs) occupy the pore space in the as-prepared framework materials. In 2004, Morris *et al.* introduced the ionothermal route as an alternative method for preparing zeolitic and other porous materials.[4-5] Ionothermal synthesis uses ionic liquids (ILs) as both the solvent and the SDA in crystallization reaction, avoiding competition between the template-framework and solvent-framework interactions that is normally present in hydrothermal or solvothermal synthesis. Another important characteristic of ionic liquids is their low vapor pressure, which leads to a much safer procedure.[4] Cooperative structure-directing agents (co-SDAs) such as organic amines or quaternary ammonium ions can be used in the ionothermal approach in a synthetic strategy offering different chemistry as a new avenue to prepare structural variety and new porous materials. Several zeolitic phosphate frameworks have been synthesized using this technique.[6-13] Amazingly, the first 20-ring extra-large-pore aluminophosphate zeotype DNL-1 with -CLO topology[14] and cobalt-substituted aluminophosphates with -CLO structure (CoDNL-1) were prepared by this method.[15]

Iron aluminophosphates (FeAPOs) are extensively studied mainly due to their potential as catalysts for hydrocarbon conversion and oxidation combustion reactions, as well as their ability to act as selective absorbents.[16-35] Chabazite (CHA) type FeAPO-34 is an interesting material because it is one of the selective catalysts used in the methanol-to-olefin (MTO) process.[36,37] FeAPO-34 is traditionally prepared under hydrothermal conditions using fluoride medium and

piperidine as the SDA, as reported by Ristic *et al.* in 2002. [38] Recently, Yang *et al.* in 2021[35] reported the solvent-free synthesis of CHA-type FeAPO-44 containing cyclohexylamine as the SDA. However, the pores of the mechanochemical material also contained ammonium citrate from the ammonium ferric citrate used as the iron source. To date there have been no published reports of the ionothermal synthesis of FeAPO-34, despite the fact that ionothermal synthesis offers a safer alternative route with low vapour pressure (compared to the high vapour pressure of hydrothermal and solvothermal syntheses). In this present work, we report the ionothermal synthesis of FeAPO-34 using 1-ethyl-3-methylimidazoliumchloride (EMIMCl) (Figure 1a) and show the need for ethylenediamine (EDA) (Figure 1b) as a co-SDA in order to allow Fe to be incorporated into the phosphate framework.

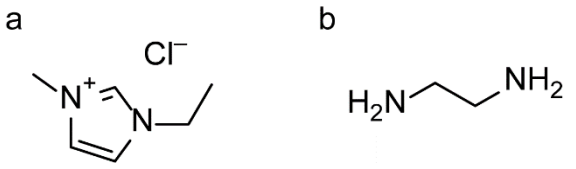

Figure 1. Structures of (a) 1-ethyl-3-methylimidazoliumchloride (EMIMCl) and (b) ethylenediamine

Materials and Methodology

Ionothermal synthesis of FeAPO-34

A Teflon-lined autoclave (23 ml) was charged with $Al[OCH(CH_3)_2]_3$ (0.1899 g, Alfa Aesar, 98%), H_3PO_4 (0.474 g, Sigma Aldrich, 99%), HF (70 µl, 3.4 mmol, Alfa Aesar. 98%), EMIMCl (4g, 27.2 mmol, Sigma Aldrich, 98%), $Fe(C_2H_3O_2)_2$ (0.122 g, 0.7 mmol, Sigma Aldrich, 95%) and ethylenediamine (0.1 g, 1.6 mmol, Sigma Aldrich, 99%). Subsequently the autoclave was heated at 210 ° C for 3 days in the oven and then cooled to room temperature. The brown

product was filtered, washed thoroughly with distilled water and methanol, and finally dried at room temperature. The sample was calcined at 550 °C in a closed line system connected to vacuum pumping until reaching 10^{-4} mbar internal pressure with heating and cooling rates of 1 K min^{-1}.

Characterization

Powder X-ray diffraction (PXRD) patterns were collected using a STOE STADI-P diffractometer operated with monochromated Cu $K\alpha_1$ radiation (λ= 1.5406 Å). Scanning electron microscopy (SEM), using a JEOL JSM 5600 was used to characterise the morphology of the crystallites. The integrated energy-dispersive X-ray (EDX) spectrometer of the same electron microscope was used to carry out elemental analysis. Thermogravimetric analysis (TGA) was carried out under air using a Netzsch STA 449C thermogravimetric analyser.

Solid-state magic angle spinning (MAS) NMR spectra were recorded using a Bruker Avance III spectrometer equipped with a 14.1 T wide-bore superconducting magnet (^{1}H Larmor frequency of 600.1 MHz). Samples were packed into 2.5, 3.2 or 4mm zirconia rotors and rotated at the magic angle at rates of 12.5-20 kHz. Solid-state ^{13}C NMR spectra were acquired at 14.1 T. Spectra were acquired using cross polarization (CP) from ^{1}H using a short contact pulse duration of 0.25 ms (ramped for ^{1}H). Two-pulse phase modulation (TPPM) ^{1}H decoupling with ν_1 ≈ 100 kHz was applied during acquisition. Signal averaging was carried out for 5120 transients with recycle intervals of 3 s. For ^{27}Al, signal averaging was carried out for 128 transients with a recycle interval of 5 s. For ^{31}P signal averaging was carried out for 1024 transients with a recycle interval of 10 s.

Static wideline ^{31}P NMR spectra were carried out to confirm isomorphic substitution of Fe in the phosphate framework. Spectra were recorded using a Bruker Avance III spectrometer equipped with a 9.4 T wide-bore superconducting magnet (^{1}H Larmor frequency of 400.1 MHz). A

radiofrequency nutation rate of ν_1 ≈180 kHz (π/2 pulse of 1.4 μs) was used, with an the echo delay of 10 μs. Frequency stepping was carried out in steps of 600 ppm (97.186 kHz), with signal averaging for 10240 transients with a recycle interval of 0.1 s for each step. Each individual step was Fourier transformed and phase corrected, then all processed spectra were coadded to provide the final spectra shown.

Result and Discussion

Powder X-ray Diffraction (PXRD) pattern as-synthesized of FeAPO-34

Figure 2 illustrates the PXRD pattern of as-synthesized triclinic CHA structure of FeAPO-34. The experimental pattern is in excellent agreement with the simulated pattern, demonstrating that FeAPO-34 is analogous to the triclinic CHA structure of AlPO-34 (Figure 2, the inset). After calcination, the template-free FeAPO-34 changes to the rhombohedral CHA structure, which can rapidly absorb atmospheric moisture. As shown in Figure 3, the PXRD pattern of the calcined, dehydrated FeAPO-34 prepared here matches very well with the pattern simulated for rhombohedral CHA-type AlPO-34 and, upon rehydration, the diffraction pattern changed markedly (consistent with the work of Tuel and co-workers,[39,40] who identified two different hydrated phases of AlPO-34, although we note that FeAPO-34 has different framework Lewis acidity so the locations of the water molecules within the pores is unlikely to be identical to the pure AlPOs.

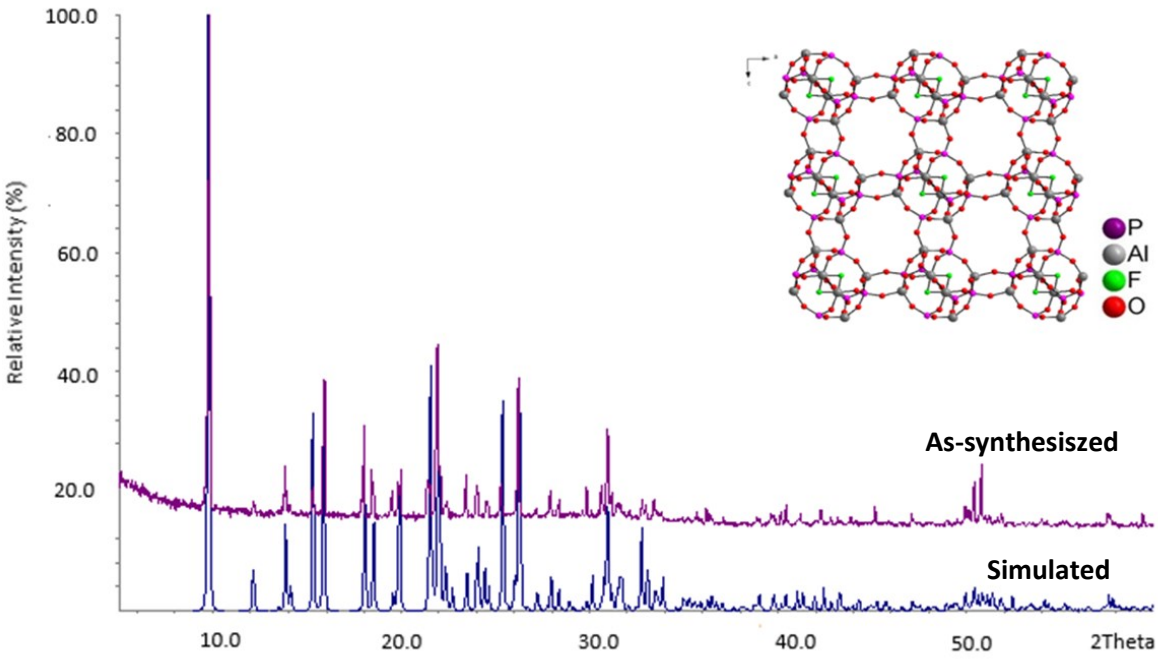

Figure 2. PXRD pattern of as-synthesized FeAPO-34 with triclinic CHA structure. The inset illustrates the CHA structure of AlPO-34 (SDA molecules are omitted).

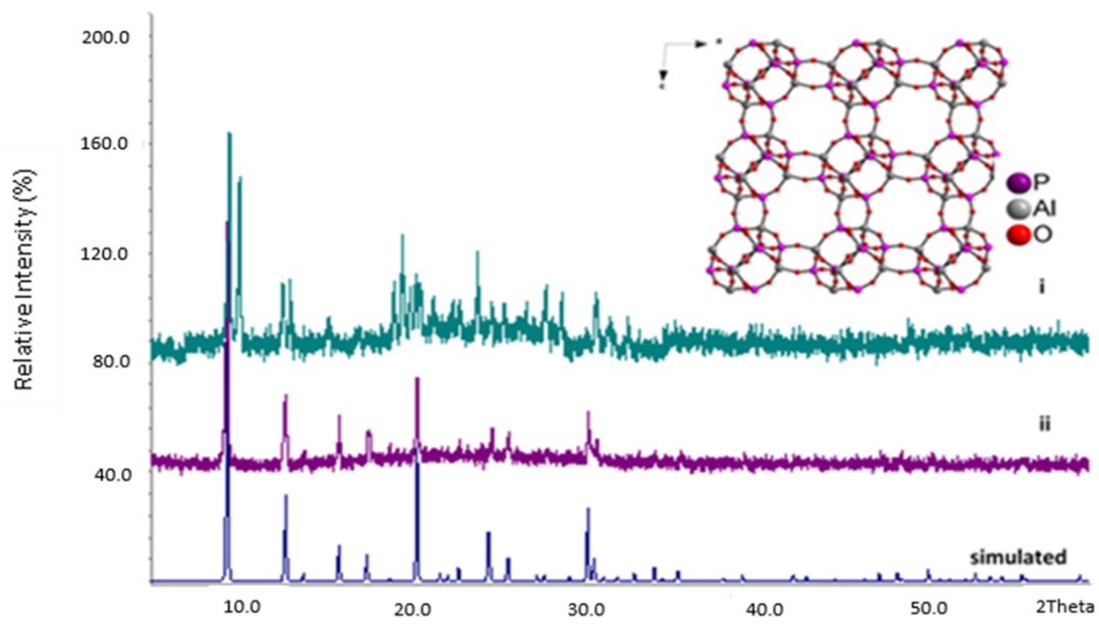

Figure 3. PXRD pattern of (i) rehydrated FeAPO-34 (ii) dehydrated calcined FeAPO-34. The inset shows the rhombohedral CHA structure.

Morphology of FeAPO-34

Figure 4 shows scanning electron micrographs of the as-synthesised and calcined FeAPO-34, which show that there is no significant difference between these two samples. Both samples are formed of agglomerates of small particles with no consistent shape or size. The particles appear to be smaller than those reported for mechanochemical or hydrothermal synthesis procedures.[35,38]

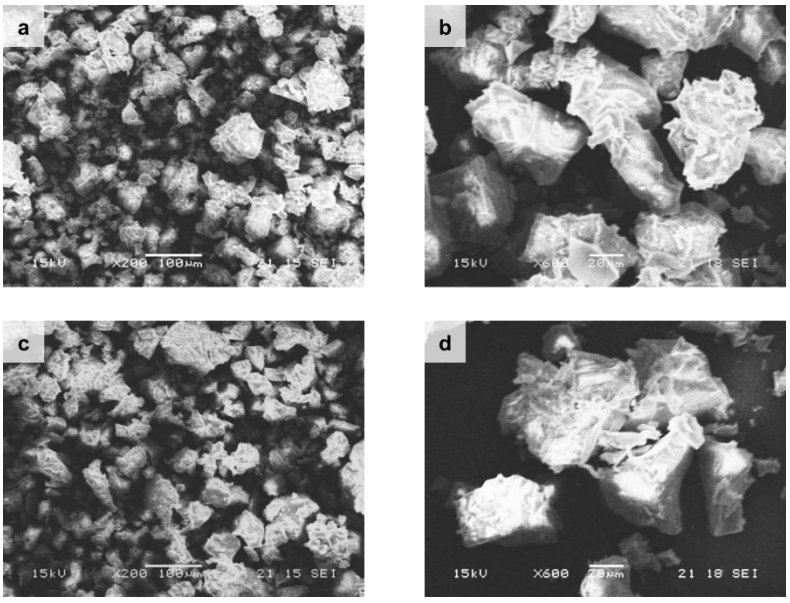

Figure 4. Scanning electron micrographs showing the particle morphology of ionothermal FeAPO-34; (a and b) as-synthesised (a) 200× and (b) 600×; (c and d) calcined (c) 200× and (d) 600× magnification.

^{13}C CP/MAS NMR of FeAPO-34

Figure 5 (a) shows the ^{13}C NMR spectra of EMIMCl and EDA in D_2O and Figure 5(b) shows the ^{13}C CP MAS NMR spectrum of the as-made FeAPO-34. The ^{13}C CP MAS NMR spectrum of FeAPO-34 contains three signals, which can be assigned to the 1, 3-dimethylimidazolium cation

(DMIM$^+$, inset in Figure 5(b)), which is formed *in situ* by transalkylation reactions within the IL. [5] This is identical to the case of the pure $AlPO_4$ analogue, SIZ-4, prepared in 1-butyl-3-methylimidazolium chloride: the butyl groups are too large to be incorporated into the pores and, instead, the DMIM$^+$ cations are observed in the crystal structure. The ^{13}C CP MAS NMR spectrum of SIZ-4[41] is shown in red in Figure 5(b) (note that the molecule is chemically symmetric but in a crystallographically asymmetric location, such that the two methyl groups give rise to distinct resonances). In the ^{13}C CP MAS NMR spectrum of FeAPO-34, all resonances are significantly broader than for SIZ-4, which is consistent with both the more compositionally disordered FeAPO-34 framework and the enhanced transverse relaxation expected for a paramagnetic material. The signal at 37 ppm is assigned to the N-methyl groups, C3, the resonance at 126 ppm is assigned to C2 and the remaining signal at 134 ppm arises from C1. From Figure 5(a), it can be seen that the ^{13}C signal for EDA would fall almost exactly under the signal for C3 of DMIM, such that it cannot be determined from the spectrum in Figure 5(b) whether EDA is present within the pores of the material. Bidentate amine ligands have recently been used in the preparation of FeAPOs, leading to the formation of octahedral FeO_4N_2 environments.[34] In such a situation, the paramagnetic relaxation enhancement for the ^{13}C signals of the amine ligand would likely render them invisible in the CP MAS experiment used here.

The general formula of the as-made FeAPO-34 can be written as $[Fe_xAl_{1-x}PO_4]_6F_2R_2$, where R is the SDA.[42] EDX analysis of the ionothermal FeAPO-34 indicated an iron content of ~2.7 mol% (x = 0.08). As mentioned above, it is unclear from ^{13}C NMR analysis whether any EDA is present in the final product. This can be investigated by CHN analysis, which revealed the material is 11.36% C, 1.56% H and 5.62% N, which corresponds to a maximum of 10% of the SDA being EDA rather than DMIM. We therefore write the idealised formula for the ionothermal FeAPO-34 as $[Fe_{0.08}Al_{0.92}PO_4]_6F_2 \cdot [C_5H_9N_2]_2$. This formula suggests that the DMIM$^+$ plays an

important role in directing the structure of the CHA-type framework and filling the pore space in the as-made material, whereas the EDA plays a more important role in the solution phase, facilitating the solubility and subsequent incorporation of Fe^{2+} into the FeAPO-34 framework. As evidence of this role, when EDA was omitted from the reaction mixture, white crystals of AlPO-34 were preferentially obtained as the product.

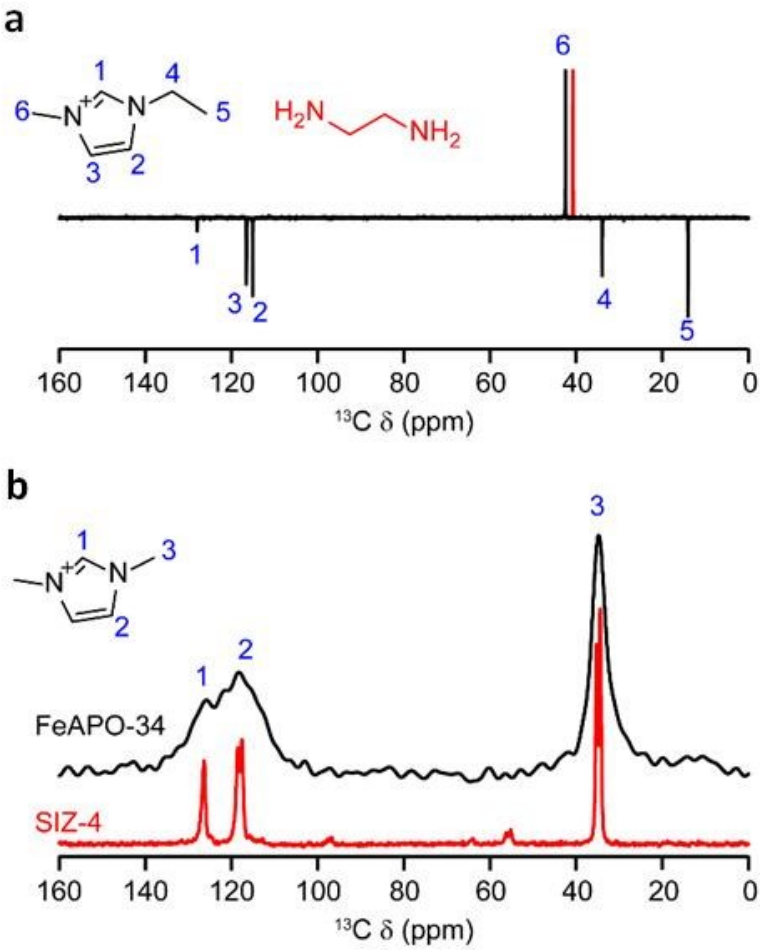

Figure 5. (a) ^{13}C (7.05 T, D_2O, DEPTQ) NMR spectra of EMIMCl (black) and EDA (red). Molecular structures are inset and show the atomic numbering scheme for $EMIM^+$. (b)^{13}C (14.1 T, 12.5 kHz CP MAS) NMR spectrum of as-made FeAPO-34 (black), overlaid with (in red) a comparable ^{13}C CP MAS NMR spectrum of the CHA-type AlPO, SIZ-4,[41] which contains dimethylimidazolium ($DMIM^+$, shown in the inset along with the corresponding atomic numbering scheme).

Thermogravimetric Analysis (TGA) of FeAPO-34

Thermogravimetric analysis (TGA) of as-synthesized FeAPO-34 material was carried out from room temperature to 650 °C. Figure 6 shows that the mass loss can be roughly separated into two steps. The first step, of 6.2% between 25 to 250 °C is due to the removal of water: below 100 °C, this water is likely physisorbed on the particle surface, but as-made phosphate-based CHA frameworks have been shown to contain water within the pores, which may be lost at higher temperatures.[43] Approximately 20.0% of the mass loss appears between 250-550 °C and this can be attributed to the loss of 1,3-dimethylimidazolium fluoride (DMIMF). A loss of one mole of DMIMF per $[Fe_{0.08}Al_{0.92}PO_4]_6$ would give a mass loss of 19.7%.[38]

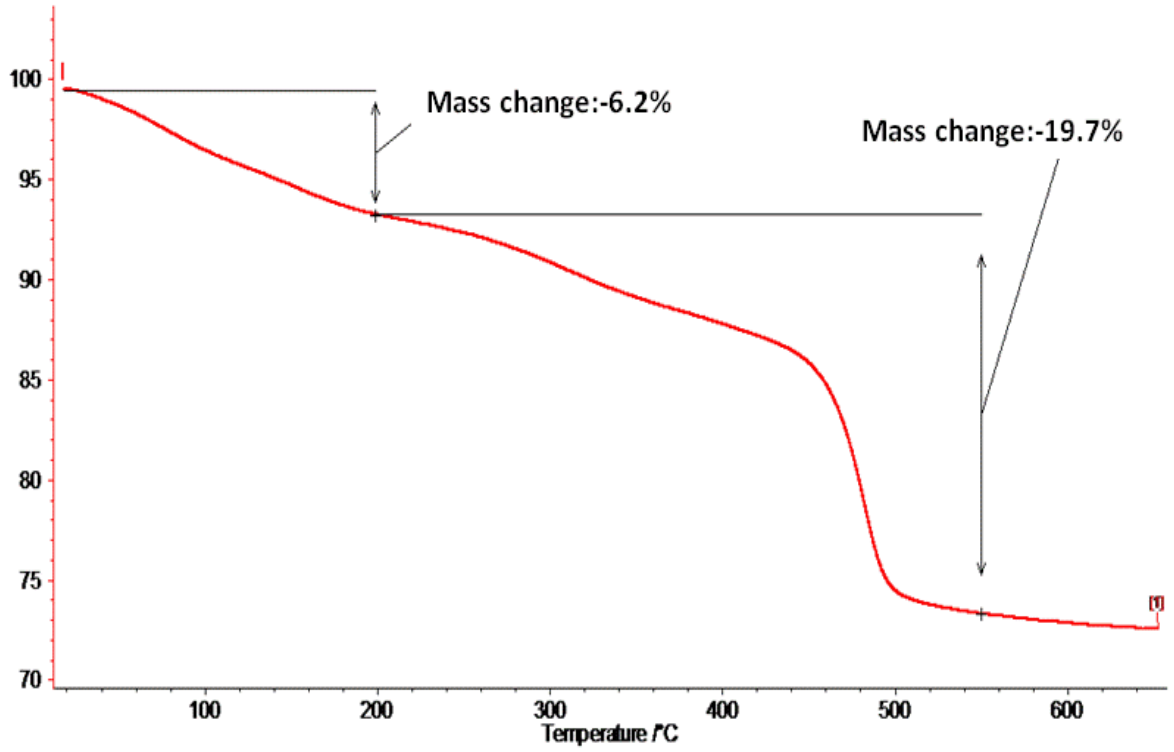

Figure 6. The TG curve of as-synthesised of FeAPO-34

^{27}Al MAS NMR of FeAPO-34

Figure 7(a) shows the ^{27}Al MAS NMR of as-synthesised FeAPO-34, which contains the expected signals for tetrahedral $Al(OP)_4$ (*ca.* 45 ppm) and octahedral $Al(OP)_4F_2$ (*ca.* –6 ppm) coordination environments.[42,44] The fluoride ions present in the material framework balance the charge of cationic SDA, which is located in the CHA cage of the material.[39] Upon calcination (Fig. 7(b)) the resonance from the octahedral Al disappears indicating that the bond between aluminium and two fluorines has been destroyed.[4] Only a single signal is observed with isotropic chemical shift, δ_{iso} = 39.5(2) ppm, quadrupolar coupling constant, C_Q = 2.8(1) MHz and quadrupolar asymmetry, η_Q = 0.9(1), corresponding to the single tetrahedral $Al(OP)_4$ site expected for the rhombohedral CHA structure of dehydrated FeAPO-34. As shown in Figure 8, the EDX spectrum of the calcined FeAPO-34 confirms that there is no Fluorine present.

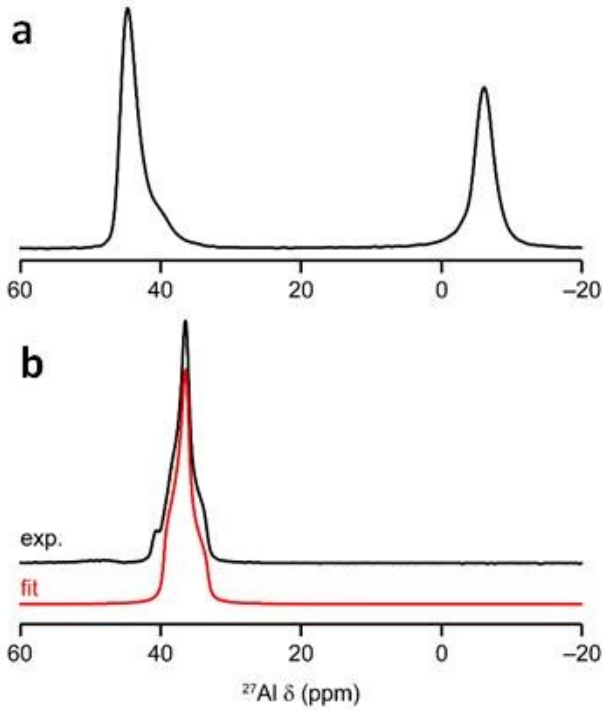

Figure 7. ^{27}Al (14.1 T) MAS NMR of (a) as-synthesized FeAPO-34 (14 kHz MAS) and (b) dehydrated FeAPO-34 (20 kHz MAS).

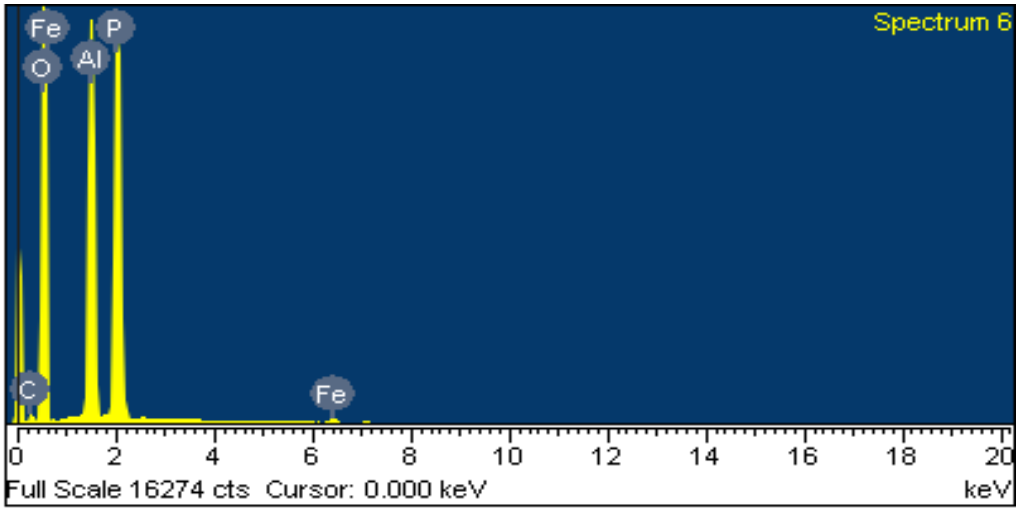

Figure 8. EDX spectra of calcined FeAPO-34.

^{31}P NMR spectroscopy of FeAPO-34

The ^{31}P MAS NMR spectrum of as-made FeAPO-34, shown in Figure 9(a), contains three resonances at –7.6, –22.7 and –28.8 ppm, corresponding to the three crystallographic P sites in tetrahedral $P(OAl)_4$ of triclinic AlPO-34 (P1, P3 and P2, respectively in the numbering scheme of Dawson *et al.*[43] The very low field resonance at -7.6 ppm is attributed to the phosphorus nearest the fluoride bridges in the structure (P1).[4,44] The ^{31}P chemical shifts in AlPO-34 also have been shown to be sensitive to the presence of different guest molecules within the framework, with P1, P2 and P3 having ranges of at least 1.2, 3.5 and 2.6 ppm, respectively, in work by Dawson *et al.*, who characterised the framework containing $DMIM^+$, $EMIM^+$, pyridine, piperidine, morpholine and cyclam. The ^{31}P chemical shifts for as-made FeAPO-34 are remarkably close to those of AlPO-34 containing $DMIM^+$ (–7.6, –22.4 and –28.6 ppm) and in significantly poorer agreement with those of AlPO-34 containing $EMIM^+$ (–7.7, –23.5 and –29.0 ppm), serving as further evidence that the as-made ionothermal FeAPO-34 contains $DMIM^+$ rather than $EMIM^+$ within the pores. The ^{31}P spectrum of the as-made FeAPO-34 also contains a broader signal that can be approximated by a single Gaussian lineshape at *ca*. –11 ppm, corresponding to amorphous phosphates that are often observed as impurities in as-made phosphate materials. It

should be noted that the broad signal displayed a spinning sideband manifold spanning ~700 ppm (not shown), which indicates the presence of iron within the amorphous phase. After calcination, the amorphous phosphate and fluorine is removed, therefore, the ^{31}P MAS NMR spectrum of the calcined, dehydrated FeAPO, shown in Figure 9(b) contains only a single sharp resonance at –30.2 ppm, attributed to the one type of $P(OAl)_4$ tetrahedral environment expected for calcined AlPO-34.[41, 45]

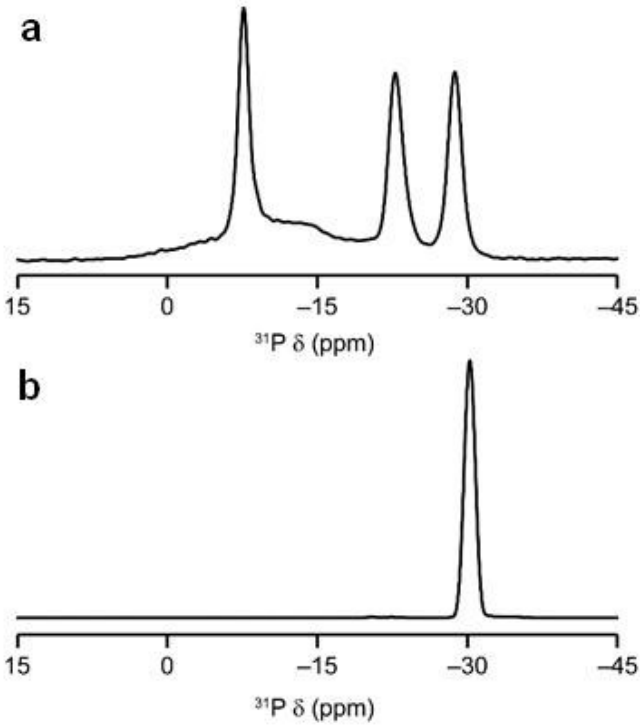

Figure 9. ^{31}P (14.1 T, 14 kHz MAS) NMR spectra of (a) as-synthesized and (b) calcined, dehydrated FeAPO-34.

Given the presence of paramagnetic Fe within the framework (confirmed by EDX spectroscopy), it is remarkable that the MAS NMR spectra reported above are so consistent with diamagnetic as-made AlPO-34 containing $DMIM^+$, and calcined, dehydrated AlPO-34. However, as previously noted by Mali *et al.*[46] and in our earlier work on the analogous ionothermal CoAPO-34,[10] the effect of the presence of M-O-P linkages (M is a paramagnetic metal ion; Ni, Co, Fe, Fe, Mn), is to broaden and shift the ^{31}P signal to the extent that it is invisible in conventional MAS NMR spectra. The signal for $P(OFe)_x(OAl)_{4-x}$ ($1 \leq x \leq 4$) can be observed using static spin echo mapping, in which the spectrum is recorded in a series of sub-spectra with evenly spaced frequency offsets. The subspectra are then summed to reconstruct the full spectrum (although, as described in further detail by Mali *et al.*, these spectra cannot be considered to be quantitative for a variety of reasons.[46] Figures 10(a) and 10(b) show the static ^{31}P spin echo mapped NMR spectra of the as-made and calcined FeAPO-34, in which a broad signal can be observed extending from around 0 ppm up to around 1.4×10^4 ppm in both cases. The shift of broadline ^{31}P NMR signal of FeAPO-34 is proportional to the electronic density of Fe atoms on the P nucleus, where the signal will shifted towards downfield in the order of $P(OAl)(OFe)_3 > P(OAl)_2(OFe)_2 > P(OAl)_3(OFe)$.[46]

Assuming a random distribution of Fe and Al, it can be calculated that in an $Al_{0.92}Fe_{0.08}PO_4$ framework, one would expect 71.64% of the P atoms to have no P-O-Fe linkages. Of the remaining 28.36% of the P atoms (*i.e.*, the ones contributing to the broad signal), 24.92% would be expected to have one P-O-Fe linkage and 3.25% would have two P-O-Fe linkages, and 0.19% would have three such linkages ($P(OFe)_4$ would be present at negligible concentration). As such, for the FeAPO-34 prepared here, one would expect to observe $P(OFe)(OAl)_3$ and $P(OFe)_2(OAl)_2$ in a 7.7 : 1 intensity ratio in a truly quantitative spectrum. In the spectra shown in Figure 10, one would expect the lineshapes to be dominated by the contribution from $P(OFe)(OAl)_3$. Furthermore, we note that, unlike in the case of aluminosilicate zeolites, where

the ^{29}Si NMR signals for $Si(OSi)_{4-x}(OAl)_x$ vary in position almost linearly with the value of n, the ^{31}P NMR signals for $P(OAl)_{4-x}(OFe)_x$ will have a more complicated distribution. For example, for x = 1, the ^{31}P will be coupled to either a S = 2 spin system (Fe^{II}) or S = 5/2 (Fe^{III}), whereas for x = 2, the ^{31}P will be coupled to S = 4 (Fe^{II}+Fe^{II}), S = 9/2 (Fe^{II}+Fe^{III}) or S = 5 (Fe^{III}+Fe^{III}) spin systems, leading to isotropic paramagnetic shifts of many tens or hundreds of thousands of ppm and linewidths on a similar order of magnitude.

While the paramagnetic interaction differs from the chemical shift interaction in its fundamental mechanism, its effect on the NMR spectrum can be modelled as a very large chemical shift-like interaction, with the peak described by its isotropic shift, δ_{iso}, width (or span, Ω), and shape (or skew, κ). Using some justifiable assumptions about typical FeAPOs, Mali *et al.* predicted "rule of thumb" paramagnetic shift parameters for $P(OFe)(OAl)_3$ with iron in the Fe^{2+} (S = 2) and Fe^{3+} (S = 5/2) oxidation states. Figure 10(c) shows the simulated chemical shift-like lineshapes for $P(OFe^{2+})(OAl)_3$ and $P(OFe^{3+})(OAl)_3$ using the parameters predicted by Mali *et al.* (note that for an interaction with a single Fe ion, the interaction should be axial, with $\kappa = \pm 1$, but when more than one spin centre contributes to the interaction, the lineshape may vary).[46] The width of the simulated lines is in surprisingly good agreement with the experimental spectra, with $P(OFe^{2+})(OAl)_3$ linkages leading to ^{31}P signal up to around 8900 ppm, and $P(OFe^{3+})(OAl)_3$ linkages leading to signal up to around 12400 ppm. It is interesting to note that, using the parameters suggested by Mali *et al.*, the lower shift ends of the signals for $P(OFe^{2+})(OAl)_3$ and $P(OFe^{3+})(OAl)_3$ are almost coincident at around 1500 ppm. Using the widths of these simulated lineshapes as a guide, the static ^{31}P NMR spectrum of the as-made FeAPO-34 has contributions from both $P(OFe^{2+})(OAl)_3$ and $P(OFe^{3+})(OAl)_3$, whereas the calcined FeAPO-34 appears to contain significantly more $P(OFe^{3+})(OAl)_3$, suggesting that the charge balancing mechanism is predominantly oxidation of the iron to Fe^{3+} (*i.e.*, isovalent substitution for Al^{3+}) rather than the formation of Brønsted acid sites (*i.e.* aliovalent substitution of Fe^{2+} + H^+ for Al^{3+}).

This observation is consistent with the work of Kaučič and co-workers, [46,47] who used wideline ^{31}P NMR and X-ray absorption spectroscopy to identify approximately equimolar Fe^{2+} and Fe^{3+} in as-made (hydrothermal) FeAPO-34, but only Fe^{3+} in the calcined material. Earlier work by Bruckner *et al.* used electron paramagnetic resonance (EPR) and Mössbauer spectroscopies to identify a similar oxidation of Fe^{2+} to Fe^{3+} upon calcination in the AFI-type FeAPO-5.[48] This behaviour is in contrast to FeAPOs with the ACO and LAU structure types, which were observed to contain only Fe^{2+} in the as-made forms. [21,24]

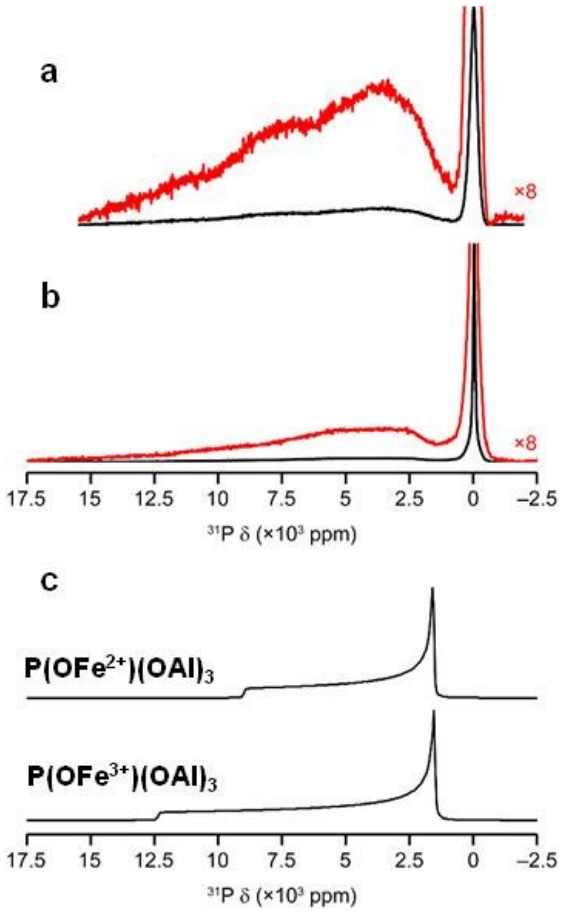

Figure 10. Static (9.4 T) ^{31}P NMR spectra of (a) as-made and (b) calcined FeAPO-34. Eight-fold vertical expansions are shown in red to highlight the presence of the broader $P(OFe)_x(OAl)_{4-x}$ signals. (c) Spectra simulated for $P(OFe^{2+})(OAl)_3$ and $P(OFe^{3+})(OAl)_3$ using the parameters predicted by Mali *et al.*[46]: $P(OFe^{2+})(OAl)_3$ δ_{iso} = 3980 ppm, Ω = 4970 ppm, κ = –1.0; $P(OFe^{3+})(OAl)_3$ δ_{iso} = 5800 ppm, Ω = 7250 ppm, κ = –1.0.

Conclusions

FeAPO-34 with CHA topology has been successfully prepared using an ionothermal synthesis route, with 1-ethyl,3-methylimidazolium ($EMIM^+$) chloride as the ionic liquid and with 1,2-diaminoethane (EDA) added as a co-template. ^{13}C NMR spectroscopy confirmed that the $EMIM^+$ cations undergo transalkylation to 1,3-dimethylimidazolium ($DMIM^+$), which occupies the pore volume of the as-made FeAPO-34. The role of the EDA is predominantly to facilitate the incorporation of Fe^{2+} within the framework, as evidenced by the fact that Fe incorporation did not occur in the absence of EDA. Wide-line ^{31}P NMR spectroscopy confirmed the incorporation of Fe into the framework, with the large paramagnetic shifts indicative of the presence of P-O-Fe linkages. From the positions and widths of the broad ^{31}P signals, it appears that the Fe is present as a mix of Fe^{2+} and Fe^{3+} in the as-made material, but is almost fully oxidised to Fe^{3+} upon calcination.

Acknowledgments

M.Musa would like to acknowledge Ministry of Higher Education Malaysia (MOHE) for the award of a scholarship which enabled her to undertake this work. Special thanks also go to Sultan Idris Education University, University of St Andrews and all parties involved in assisting to complete this research work.The research data supporting this publication can be accessed at https://doi.org/10.17630/d409a295-fe4d-4a2f-88ea-4c4a52f9004d.[49]

References

[1] A. Corma. Inorganic Solid Acids and Their Use in Acid-Catalyzed Hydrocarbon Reactions. *Chem. Rev.* **1995**, *95*, 559–614.

[2] M. E. Davis.; R. F. Lobo. Zeolite and Molecular Sieve Synthesis. *Chem. Mater.* **1992**, 4, 756-768

[3] A. Corma. From Microporous to Mesoporous Molecular Sieve Materials and Their Use in Catalysis. *Chem. Rev.* **1997**, *97*, 2373–2420.

[4] E. R. Cooper.; C. D. Andrews.; P. S. Wheatley.; P. B. Webb.; P. Wormald.; R.E. Morris. Ionic Liquids and Eutectic Mixtures as Solvent and Template in Synthesis of Zeolite Analogues. *Nature.* **2004**, *430*, 1012–1016.

[5] E. R. Parnham.; R. E. Morris. Ionothermal Synthesis of Zeolites, Metal–Organic Frameworks, and Inorganic–Organic Hybrids. *Acc. Chem. Res.* **2007**, *40*, 1005–1013.

[6] L. Wang.; Y. Xu.; Y. Wei.; J. Duan.; A. Chen.; B. Wang.; H. Ma.; Z. Tian.; L. Lin. Structure-Directing Role of Amines in the Ionothermal Synthesis**.** *J. Am. Chem. Soc.* **2006**, *128*, 7432–7433.

[7] R. Pei.; Y. Wei.; K. Li.; G. Wen.; R. Xu.; Y. Xu.; L. Wang.; H. Ma.; B. Wang.; Z. Tian.; W. Zhang.; L. Lin. Mixed Template Effect Adjusted by Amine Concentration in Ionothermal Synthesis of Molecular Sieves. *Dalton Trans.* **2010**, *39*, 1441–1443.

[8] M. Yang.; F. Xu.; Q. Liu.; P. Yan.; X. Liu.; C. Wang.; U. Welz-Biermann. Chelated Orthoborate Ionic Liquid as a Reactant for the Synthesis of a New Cobalt Borophosphate Containing Extra-Large 16-Ring Channels. *Dalton Trans.* **2010**, *39*, 10571–10573.

[9] E. J. Fayad.; N. Bats.; C. E. Kirschhock.; B. Rebours.; A. A. Quoineaud.; J. A. Martens. A Rational Approach to the Ionothermal Synthesis of an AlPO4 Molecular Sieve with an LTA-Type Framework. *Angew. Chem. Int. Ed.* **2010**, *49*, 4585–4588.

[10] M. Musa.; D. M. Dawson.; S. E. Ashbrook.; R. E. Morris. Ionothermal Synthesis and Characterization of CoAPO-34 Molecular Sieve. *Micropor. Mesopor. Mater.* **2017**, *239*, 336–341.

[11] H. Xing.; J. Li.; W. Yan.; P. Chen.; Z. Jin.; J. Yu.; S. Dai.; R. Xu. Cotemplating Ionothermal Synthesis of a New Open-Framework Aluminophosphate with Unique Al/P Ratio of 6/7. *Chem. Mater.*, **2008**, *20*, 4179–4181.

[12] H. Xing.; W. Yang.; T. Su.; Y. Li.; J. Xu.; T. Nakano.; J. Yu.; R. Xu. Ionothermal Synthesis of Extra-Large-Pore Open-Framework Nickel Phosphite $5\,H_3O{\cdot}[Ni_8(HPO_3)_9Cl_3]{\cdot}1.5\,H_2O$: Magnetic Anisotropy of the Antiferromagnetism. *Angew. Chem. Int. Ed.* **2010**, *49*, 2328–2331.

[13] J.-D. Feng.; K.-Z. Shao.; S.-W. Tang.; R.-S. Wang.; Z.-M. Su. Ionothermal Synthesis of a New Open-Framework Zinc Phosphite NIS-3 with Low Framework Density. *CrystEngComm*. **2010**, *12*, 1401–1403.

[14] Y. Wei.; Z. Tian.; H. Gies.; R. Xu.; H. Ma.; R. Pei.; W. Zhang.; Y. Xu.; L. Wang.; K. Li.; B. Wang.; G. Wen.; L. Lin. Ionothermal Synthesis of an Aluminophosphate Molecular Sieve with 20-Ring Pore Openings. *Angew. Chem. Int. Ed.* **2010** , *49*, 5367–5370.

[15] D. Li.; Y. Xu.; Y. Wang.; H. Liu.; B. Wang.; H. Ma.; R. Xu.; Z. Tian. Ionothermal Syntheses and Characterizations of Cobalt-Substituted Extra-Large Pore Aluminophosphate Molecular Sieves with -CLO Topology. *Micropor. Mesopor. Mater.* **2014**, *198*, 153–160.

[16] P.-S.; E. Dai.; R. H. Petty.; C. W. Ingram.; R. Szostak. Metal Substituted Aluminophosphate Molecular Sieves as Phenol Hydroxylation Catalysts. *Appl. Catal. A: Gen.* **1996**, *143*, 101–110.

[17] J. Ma.; B. Fan.; R. Li.; J. Cao. Characteristics of Fe/$AlPO_4$-5 Catalyst Prepared with Organic Solution. *Catal. Lett.* **1994**, 23, 189–194.

[18] P. Tian.; Z. Liu.; Z. Wu.; L. Xu.; Y. He. Characterization of Metal-Containing Molecular Sieves and Their Catalytic Properties in the Selective Oxidation of Cyclohexane. *Catal. Today* **2004**, *93–95*, 735–742.

[19] L. Zhou.; J. Xu.; H. Miao.; X. Li, F. Wang. Synthesis of FeCoMnAPO-5 Molecular Sieve and Catalytic Activity in Cyclohexane Oxidation by Oxygen. *Catal. Lett.* **2005**, *99*, 231–234.

[20] L. Zhou.; J. Xu.; C. Chen.; F. Wang.; X. Li. Synthesis of Fe, Co, and Mn Substituted AlPO-5 Molecular Sieves and Their Catalytic Activities in the Selective Oxidation of Cyclohexane. *J. Porous Mater.* **2008**, *15*, 7–12.

[21] Y. Guo.; X. Song.; J. Li.; Y. Li.; Y. Han.; J. Yu.; R. Xu. Syntheses and Characterizations of Heteroatom-Containing Open-Framework Aluminophosphates. *Dalton Trans.*, **2011**, *40*, 9289–9294.

[22] Y. Wang.; Y. Li.; L. Wang.; J. Zhang.; Y. Yan.; J. Li.; J. Yu.; J. Wang.; R. Xu. ACO-Zeotype Iron Aluminum Phosphates with Variable Al/Fe Ratios Controlled by F^- Ions. *Inorg. Chem*. **2011**, *50*, 1820–1825.

[23] L. Qi.; X Qi.; J. Wang.; L. Zheng. A Synergistic Effect in the Combination of H_2O_2, FeAPO-5 and NaBr for Selective Oxidation of Benzyl Alcohols. *Catal. Commun.*, **2011**, *16*, 225–228.

[24] Y. Guo.; L. Shao.; X. Song.; J. Li. Synthesis, Characterization and Template Removal of an Iron-Containing Aluminophosphate Molecular Sieve with LAU Topology. *Micropor. Mesopor. Mater.* **2013**, *165*, 14–19.

[25] F. Wang.; L. Liang.; J. Ma.; J. Sun. Synthesis of Fe Substituted Aluminophosphate FeAPO-5 Zeolite with Mesoporosity in Compressed CO_2 for the Improved Catalytic Activity. *Mater. Lett.* **2013**, *111*, 201–203.

[26] Y. Guo.; Y. Qiu.; J. Li.; L. Shao.; X. Song. Synthesis and Characterization of a New Open-Framework Mixed-Valence Aluminum–Iron Phosphate $(C_4H_{12}N_2)_2[Fe_2Al_5(PO_4)_8(H_2O)]$. *Inorg. Chem. Commun.* **2014**, *47*, 99–101.

[27] E.-P. Ng.; J.-P. Ghoy.; H. Awala.; A. Vincente.; R. Adnan.; T. C. Ling.; S. Mintova. Ionothermal Synthesis of FeAPO-5 in the Presence of Phosphorous Acid. *CrystEngComm*. **2016**, *18*, 257–265.

[28] H. Shao.; J. Chen.; X. Chen.; Y. Leng.; J. Zhong. Hydroxylation of Phenol Over MeAPO Molecular Sieves Synthesized by Vapor Phase Transport. *Russ. J. Phys. Chem.* **2016**, *90*, 1326–1333.

[29] Y. Luo.; X. Liang.; S. Wang.; X. Gao.; Z. Zhang.; Y. Fang. Iron Doped Aluminophosphate Molecular Sieve with Improved Adsorption Capacity for Water Vapor. *Adsorption*. **2018**, *24*, 551–561.

[30] X. Zhao.; X. Zhang.; Z. Hao.; X. Gao.; Z. Liu. Synthesis of FeAPO-5 Molecular Sieves with High Iron Contents via Improved Ionothermal Method and Their Catalytic Performances in Phenol Hydroxylation. *J. Porous Mater.* 2018, *25*, 1007–1016.

[31] X. Zhao.; Q. Wang.; W. Duan.; G. Li.; D. Ji.; Y. Shao. Synthesis of ATN-Type FeAPO-39 Molecular Sieves without Solvent using the Additional Structure-Directing Effect of the Iron Source. *Eur. J. Inorg. Chem.* **2018**, *39*, 4331–4337.

[32] X. Zhao.; W. Duan.; X. Zhang.; D. Ji.; Y. Zhao.; G. Li. React Insights into the Effects of Modifying Factors on the Solvent-Free Synthesis of FeAPO-5 Catalysts Towards Phenol Hydroxylation. *Kinet. Mech. Cat*. **2018**, *125*, 1055–1070.

[33] A. Papageorgiou.; K. S. K. Reddy.; D. Karonis.; D. Reinalda.; Y. Al Wahedi.; G. N. Karanikolos. Morphology, Activation, and Metal Substitution Effects of $AlPO_4$-5 for CO_2 Pressure Swing Adsorption. *Frontiers Chem.* **2020**, *8*, 568669.

[34] A. E. Watts.; M. M. Lozinska.; A. M. Z. Slawin.; A. Mayoral.; D. M. Dawson.; S. E. Ashbrook.; B. E. Bode.; A. I. Dugulan.; M. D. Shannon.; P. A. Cox.; A. Turrina.; P. A. Wright. Site-Specific Iron Substitution in STA-28, a Large Pore Aluminophosphate Zeotype Prepared by Using 1,10-Phenanthrolines as Framework-Bound Templates. *Angew. Chem. Int. Ed.* **2020**, *24*, 15186–15190.

[35] Z. Yang.; D. Wang.; D. Ji.; G. Li.; X. Zhao. Solvent-Free Synthesis of FeAPO-44 Molecular Sieves with CHA Structures. *Solid State Sci.* **2021**, *119*, 106698.

[36] G. F. Froment.; W.J.H. Dehertog.; A. J. Marchi. Zeolite Catalysis in the Conversion of Methanol into Olefins. *Catalysis*. **1992**, 9, 1-64.

[37] A. Tuel.; I. Arčon.; N. N. Tušar.; A. Meden.; V. Kaučič. EXAFS and NMR Investigation of Zinc, Manganese and Cobalt Substituted Aluminophosphates with the Chabazite Structure. *Micropor. Mater.* **1996**, *7*, 271–284.

[38] A. Ristić.; N. N. Tušar.; I. Arčon.; F. Thibault-Starzyk.; D. Hanžel.; J. Czyzniewska.; V. Kaučič.; Synthesis and Characterization of Triclinic MeAPO-34 (Me=Zn, Fe) Molecular Sieves. *Micropor. Mesopor. Mater.* **2002**, *56*, 303–315.

[39] A. Tuel.; S. Caldarelli.; A. Meden.; L. B. McCusker.; C. Baerlocher.; A. Ristic.; N. Rajic.; G. Mali.; V. Kaucic. NMR Characterization and Rietveld Refinement of the Structure of Rehydrated $AlPO_4$-34. *J. Phys. Chem. B*. **2000**, *104*, 5697–5705.

[40] G. Poulet.; P. Sautet.; A. Tuel. Structure of Hydrated Microporous Aluminophosphates: Static and Molecular Dynamics Approaches of $AlPO_4$-34 from First Principles Calculations. *J. Phys. Chem. B*. **2002**, *106*, 8599–8608.

[41] J. M. Griffin.; L. Clark.; V. R. Seymour.; D. W. Aldous.; D. M. Dawson.; D. Iuga.; R. E. Morris.; S. E. Ashbrook. Ionothermal ^{17}O enrichment of Oxides using Microlitre Quantities of Labelled Water. *Chem. Sci.* **2012**, *3*, 2293–2300.

[42] N. Rajić.; A. Ristić.; A. Tuel.; V. Kaučič. A CoAPO-34 Derived from a Triclinic Precursor Prepared in the Presence of HF. *Zeolites*. **1997**, *18*, 115–118.

[43] D. M. Dawson.; J. M. Griffin.; V. R. Seymour.; P. S. Wheatley.; S. E. Ashbrook.; M. Amri.; R. I. Walton.; N. Guillou.; T. Kurkiewicz.; S. Wimperis. A Multinuclear NMR Study of Six Forms of AlPO-34: Structure and Motional Broadening. *J. Phys. Chem. C*, **2017**, *121*, 1781–1793.

[44] Z. Yan.; B. Chen.; Y. Huang. A solid-state NMR Study of the Formation of Molecular Sieve SAPO-34. *Solid State Nucl. Magn. Reson.* **2009**, *35*, 49–60.

[45] A. Brückner.; U. Lohse.; H. Mehner. The Incorporation of Iron Ions in $AlPO_4$-5 Molecular Sieves After Microwave Synthesis Studied by EPR and Mössbauer Spectroscopy. *Micropor. Mesopor. Mater.* **1998**, *20*, 207–215.

[46] G. Mali'.; A. Ristić.; V. Kaučič. ^{31}P NMR as a Tool for Studying Incorporation of Ni, Co, Fe, and Mn into Aluminophosphate Zeotypes. *J. Phys. Chem. B*. **2005**, *109*, 10711–10716.

[47] I. Arčon.; A. Ristić.; N. Novak Tušar.; V. Kaučic. XAS Investigation of Iron Substitution in Triclinic FeAPO-34. *Physica Scripta*. **2005**, *T115*, 753–755.

[48] N. N. Tušar, V. Kaučič, S. Geremia and G. Vlaic, *Zeolites*, 1995, **15**, 708-713.

[49] M. Musa, D. M. Dawson, R. E. Morris and S. E. Ashbrook, **2022**, Data underpinning: "Synthesis of FeAPO-34 Molecular Sieve under Ionothermal Condition". Dataset. University of St Andrews Research Portal. https://doi.org/10.17630/d409a295-fe4d-4a2f-88ea-4c4a52f9004d